Charge-to-Mass Ratio for the Electron

Anusha Fatima Alam (1009056539) and Tanvi Kaur Manku (1009075313)

November 22, 2023

1 Introduction [1]

The primary objective of this lab is to experimentally determine the charge-to-mass ratio of an electron and to explore the factors that influence the behaviour of charged particles inside a magnetic field. By considering a variation of the J.J. Thompson's original experiment, the charge-to-mass ratio can be determined by observing the radius of the electron beam as electrons are emitted from a hot filament and move through a magnetic field generated by a pair of Helmholtz coils.

An electron of charge e and mass m moving with velocity $\vec{v}$ inside magnetic field $\vec{B}$ experiences magnetic force $\vec{F} = e\vec{v} \times \vec{B}$. The electron moves in circular orbit with radius r if $\vec{B}$ is constant and $\vec{v}$ is perpendicular to $\vec{B}$. By Newton's second law, this magnetic force provides centripetal acceleration $\frac{v^2}{r}$.

$$evB = m\frac{v^2}{r} \tag{1}$$

The work done by the field on the electron moving through a potential difference ΔV is given by:

$$e\Delta V = \frac{1}{2}mv^2 \tag{2}$$

By rearranging Equations 1 and 2 and eliminating v^2, the curvature of the electron orbit is determined.

$$\frac{1}{r} = \sqrt{\frac{e}{2m}}\frac{B}{\sqrt{\Delta V}} \tag{3}$$

The total axial magnetic field $\vec{B}$ consists of two characteristic fields: the external magnetic field from the surroundings given by $\vec{B_e}$ and the magnetic field generated by the pair of Helmholtz coils $\vec{B_c}$ such that this field is uniformly approximated as $\vec{B_c} = (\frac{4}{5})^{\frac{3}{2}}\frac{\mu_0 nI}{R}$. Therefore:

$$\vec{B} = \vec{B_c} + \vec{B_e} \rightarrow B = B_c + B_e \tag{4}$$

$$B = (\frac{4}{5})^{\frac{3}{2}}\frac{\mu_0 nI}{R} + B_e \tag{5}$$

where μ_0 is the permeability of free space ($\mu_0 = 4\pi \cdot 10^{-7}\ \mathrm{T \cdot m \cdot A^{-1}}$), and I and R is the current and radius of the Helmholtz coil respectively.

Substituting equation 5 into equation 3 and defining the characteristic dimension of the coil, k, and I_0 a constant:

$$k = \frac{1}{\sqrt{2}}(\frac{4}{5})^{3/2}\frac{\mu_0 n}{R} \tag{6}$$

$$I_0 = \frac{B_e}{k} \tag{7}$$

The radius of curvature of an electron beam is:

$$\frac{1}{r} = \sqrt{\frac{e}{m}}k\frac{I + \frac{1}{\sqrt{2}}I_0}{\sqrt{\Delta V}} \tag{8}$$

2 Materials and Methods

2.1 Materials

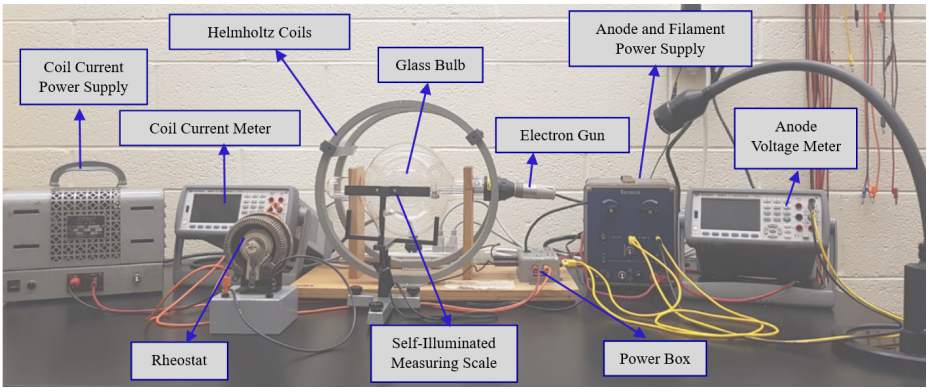

Figure 1: Annotated diagram of the experimental set-up and the apparatus.

Apparatus (refer to Figure 1 for a labelled diagram):

- Electron Gun
- Glass bulb Filled with Hydrogen Gas
- Helmholtz Coils
- Anode Voltage Meter ($\pm$ 0.0005 V)
- Coil Current Meter ($\pm$ 0.000005 A)
- Power Box
- Anode and Filament Power Supply
- Coils Power Supply
- Rheostat
- Self-Illuminated Measuring Scale with Plastic Reflector ($\pm$ 0.05 cm)

The instrumental uncertainties quoted above of the anode voltage meter, coil current meter, and self-illuminated measuring scale are not sufficient to describe the degree of uncertainty in the measured readings. For the anode voltage and coil current meter, the readings were constantly fluctuating- therefore, the degree of uncertainty is taken as the first digit that was not fluctuating to accommodate the largest source of uncertainty. Hence, the uncertainty of the anode voltage meter and coil current meter is $\pm$ 0.1 V and $\pm$ 0.001 A respectively. Similarly, an uncertainty of $\pm$ 0.1 cm was used for the self-illuminated scale because the electron path was quite diffused, and the resolution of the scale readings on the plastic reflector was too small to record a more precise reading.

2.2 Method

1. The power supply of the electron gun was turned on and was left on for 30 s to allow the filament of the electron gun to heat up.
2. The anode voltage meter, the coil current meter and the power supply for the Helmholtz coil were turned on, and the initial current and voltage were adjusted until a sharp electron beam was visible inside the glass bulb.
3. The glass bulb was rotated to ensure the electron trajectory had a smooth, vertically circular closed path, not a helix shape.
4. The radius of the circular electron beam was recorded at different coil currents at a constant accelerating potential. The radius was measured using the reflected self-illuminated measuring scale projected on the plastic reflector.
5. Step **4** was repeated with different accelerating potentials at a constant current.
6. The influence of ferromagnetic materials and other sources of magnetic fields was observed by placing such materials (like cell phones) near the glass bulb.

3 Data and Analysis [1]

The measured coil radius, R, is 16 ± 0.1 cm $= 0.16 \pm 0.001$ m, and the number of turns in each coil, n, is 130.

The experimentally measured electron path radius and current were plotted in Figure 2. The fit was found to have a slope of $-2.7 \pm 0.05 \frac{\text{cm}}{\text{A}}$ with an intercept of 7.8 ± 0.06cm. The R^2 of this fit was found to be 0.997, close to the ideal value of 1. The reduced χ^2_ν was calculated to be 0.30, closer to 0 than the ideal value of 1, implying an overfit. However, since the fit is linear (a polynomial of degree 1), it was not logical to assume that it is an overfit since choosing a fit with a lower degree would be a constant value, so the produced fit is a good fit. From Figure 3, it can be seen that all the residuals are within the uncertainty range of ± 0.1 cm of r. Therefore, the produced fit for the relationship between electron path radius and coil current is good.

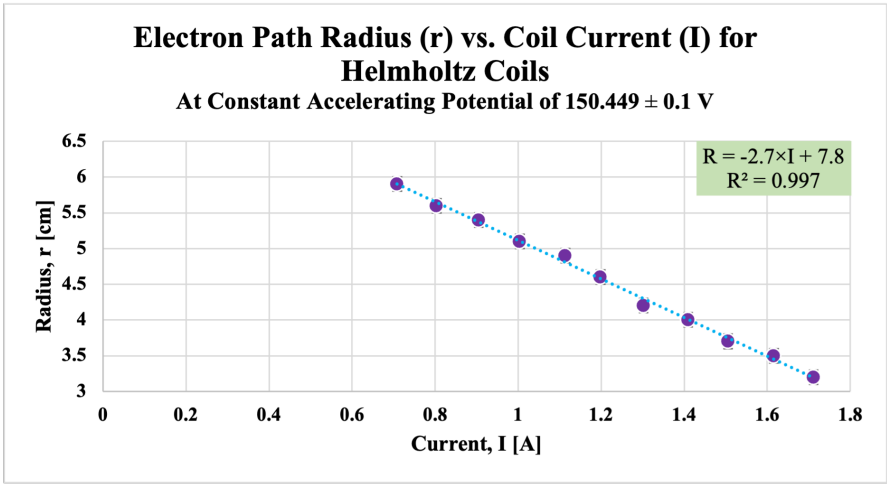

Figure 2: Scatter plot of electron path radius, r, against coil current, I, at a constant acceleration potential of 150.449 ± 0.1 V, with a linear fit represented by the blue dotted line. The black error bars are barely visible but are based on reading uncertainty, which is 0.001 A for I and 0.1 cm for r.

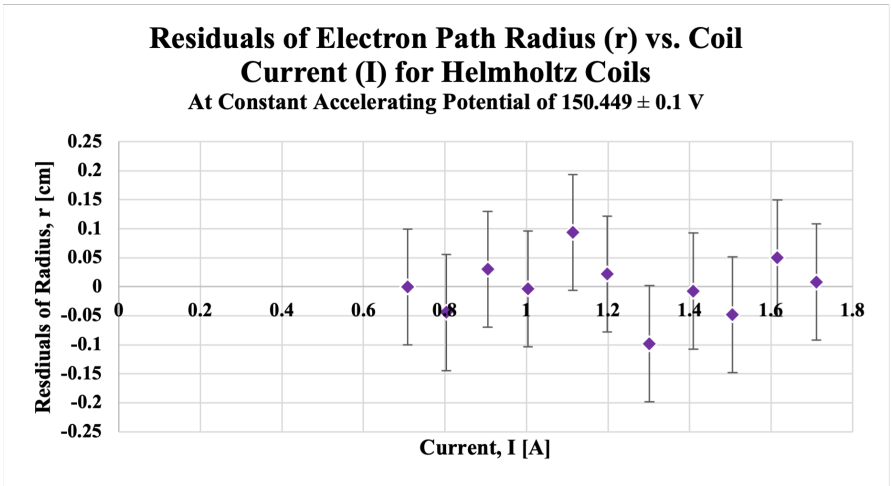

Figure 3: Scatter plot of residual electron path radius, r, against coil current, I, at a constant acceleration potential of 150.449 ± 0.1 V. The vertical error bars, in black, represent the reading uncertainty of 0.1 cm for r. The black horizontal error bars are barely visible but show the reading uncertainty of 0.001 A for I.

The experimentally measured electron path radius and accelerating potential were plotted in Figure 4. The fit was found to have a slope of $0.01 \pm 0.30 \times 10^{-3} \frac{\text{cm}}{\text{V}}$ with an intercept of 1.6 ± 0.07cm. The R^2 of this fit was found to be 0.995, close to the ideal value of 1. The reduced χ^2_ν was calculated to be 0.53, somewhat close to the ideal value 0f 1, implying a good fit. Figure 5 shows that nearly all the residuals, except for one data point near 250 V, are within the uncertainty range of ± 0.1 cm of r. However, this 'outlier' data point was near the

[1] Refer to Appendix A for experimental data in tabular format and information on plot and fit production, and calculation of χ^2_ν. Refer to Appendix B for details of error propagation and calculated data. Also note that the SI units for length are meters, m, but most length-related measurements have mostly been presented in cm for clarity.

data range, so it was included in the analysis. Therefore, the produced fit for the relationship between electron path radius and accelerating potential is good.

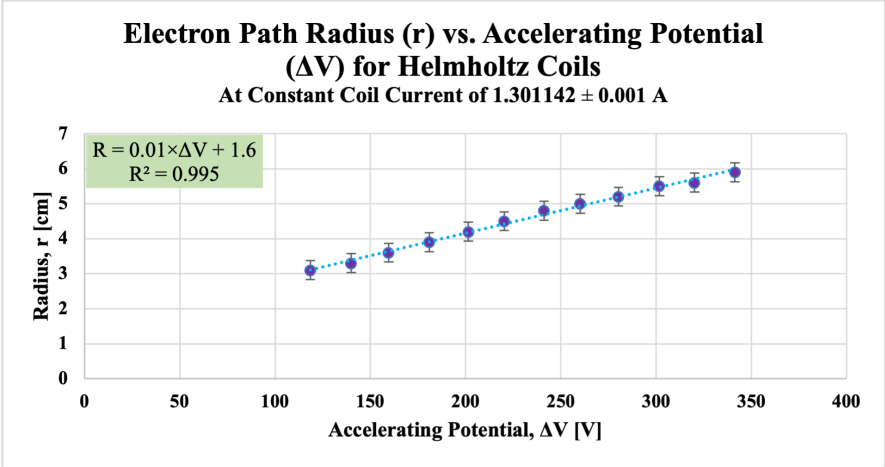

Figure 4: Scatter plot of electron path radius, r, against accelerating potential, ΔV, at a constant coil current of 1.301142 ± 0.001 A, with a linear fit represented by the blue dotted line. The vertical error bars in black represent the reading uncertainty of 0.1 cm for r. The black horizontal error bars are barely visible but are based on a reading uncertainty of 0.1 V for ΔV.

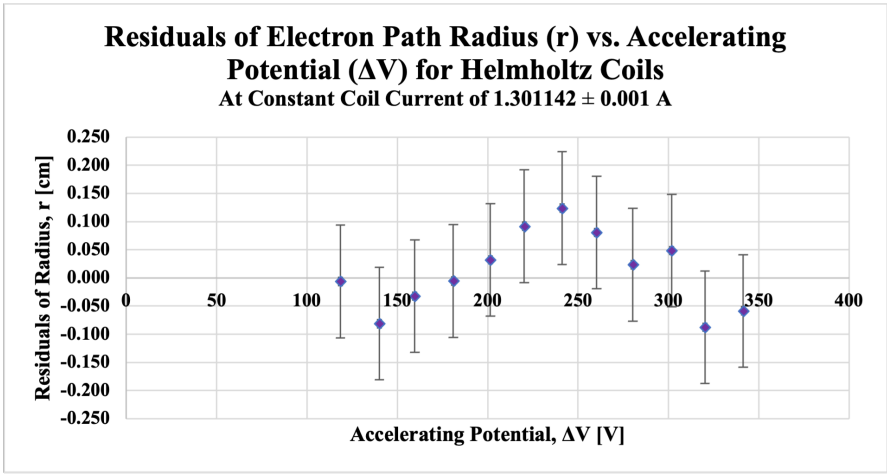

Figure 5: Scatter plot of residual electron path radius, r, against coil current, ΔV, at a constant acceleration potential of 150.449 ± 0.1 V. The vertical error bars, in black, represent the reading uncertainty of 0.1 cm for r. The black horizontal bars are barely visible but show the reading uncertainty of 0.1 V in ΔV.

4 Discussion and Conclusion

4.1 Reducing Impact of Parallax Errors

To minimize the impact of parallax errors on radius measurements, a self-illuminating measuring scale was projected on a plastic reflector and, further, onto the glass bulb to take more accurate readings by aligning the center of the reflected scale to the center of the circular trajectory formed by the electron beam. This instrument helped eliminate parallax error by providing a fixed observer perspective, reducing error due to changes in the angle between the observer and bulb. Additionally, since the scale was precisely aligned on the same plane as the glass bulb, there was no 'shift' and minimal inaccuracy in the scale's markings caused by the bulb's curvature.

4.2 Behavior of Electron Trajectory in a Strong Magnetic Field

At subsequently high coil-currents and low accelerating potential differences, a strong magnetic field $\vec{B_c}$ is generated wherein an anomalous behaviour of the electron trajectory is observed.

4.2.1 Effect on Trajectory

At relatively large coil currents and low accelerating voltage, the magnetic field is high, which causes a deviation in the typical circular path of the electron trajectory. As such, the trajectory becomes more diffused and less uniform. More specifically, certain parts of the trajectory are more affected then others because the magnetic field is not uniform, which means particular regions observe a stronger field while others observe a weaker field. This introduces uneven deflections causing the electron trajectory to become more diffused in certain regions.

4.2.2 Reduction of Error

Irregularities and lack of uniformity in the circular electron path impact the accuracy of the radius readings and, effectively, the calculated charge-to-mass ratio. This error can be minimized by optimizing the experimental parameters. This can be done by measuring within an interval of the accelerating voltage and coil current where the effect of this anomalous behaviour is negligible and measurable deflections are still observable, taking repeated measurements, improving the uniformity of the magnetic field produced by the coils, and shielding the setup from external magnetic influences.

4.2.3 Correction Factor [1]

Although the magnetic field produced by the coils is mostly constant along the axis, it does decrease away from the axis such that for off-axis distances ρ, the z-component of the magnetic field, $B(\rho)$, which is the only one considered in this experiment:

- If $\rho < 0.2R$,
$$B(\rho) \approx 99.925\% \text{ of } B(0) \tag{9}$$
- If $0.2R < \rho < 0.5R$,
$$B(\rho) \approx 1 - \frac{\rho^4}{R^4(0.6583 + 0.29\frac{\rho^2}{R^2})^2} B(0) \tag{10}$$

.

In this experiment, since the electrons are produced at a fixed point, the path is not centred at the coil axis, so the effect of distance on B must be accounted for. As the recorded radii are relatively large, using the radius, r, as the value for ρ will appropriately consider the effect of distance.

4.3 Magnetic Field not Produced by Coils, B_e

Equation 3 was substituted into 4 and isolated for the coil-produced field, B_c, to find the external field, B_e,

$$B_c = \sqrt{\frac{2m}{e}\Delta V}\frac{1}{r} - B_e \tag{11}$$

Equation 11 was used with the measured values of coil current (Figure 2) to calculate B_c, which were corrected as per Section 4.2.3. The B_c values were plotted against the inverse of experimentally measured electron path radii (Table 1), resulting in Figure 6. The fit was found to have a slope of $5.2 \times 10^{-3} \pm 0.30 \times 10^{-3}$ T $\cdot$ cm, which is the value of $\sqrt{\frac{2m}{e}\Delta V}$ and a y-intercept of $-0.32 \times 10^{-3} \pm 0.07 \times 10^{-3}$T, which is the value of the magnetic field not produced by the coils, B_e, by Equation 11. The R^2 of this fit was found to be 0.971, close to the ideal value of 1. The reduced χ^2_ν was calculated to be 0.13×10^3, much larger than the ideal value of 1, meaning an underfit, and the experimental data may be better fitted to a quadratic than a linear. From Figure 7, it can be seen that most of the residuals are only marginally larger than the uncertainty range of B_c. Therefore, the fit for the relationship between the coil-produced magnetic field and the inverse of the electron path radii is somewhat good.

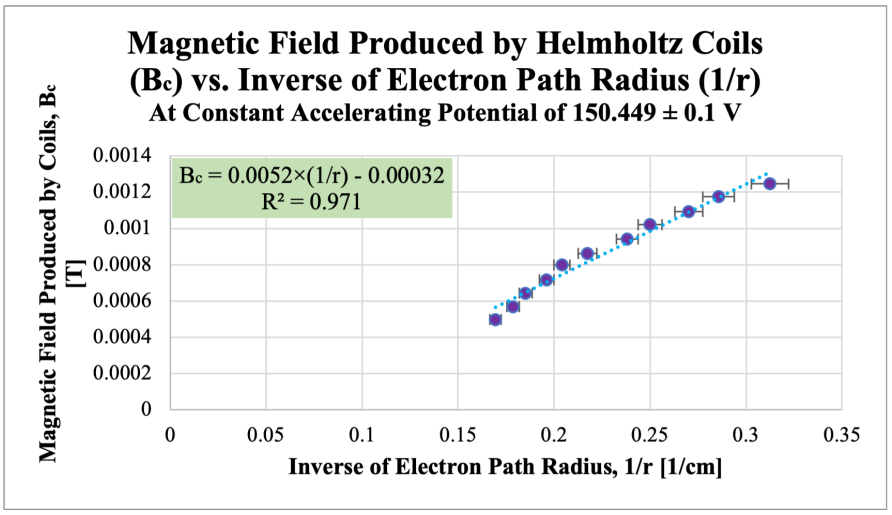

Figure 6: Scatter plot of coil-produced magnetic field, B_c against inverse of electron path radius, $\frac{1}{r}$, at a constant accelerating potential of 150.449 ± 0.1 V, with a linear fit represented by the blue dotted line. The black vertical error bars are barely visible but represent the calculated uncertainty for B_c. The black horizontal error bars represent the calculated uncertainty for $\frac{1}{r}$ (Table 4).

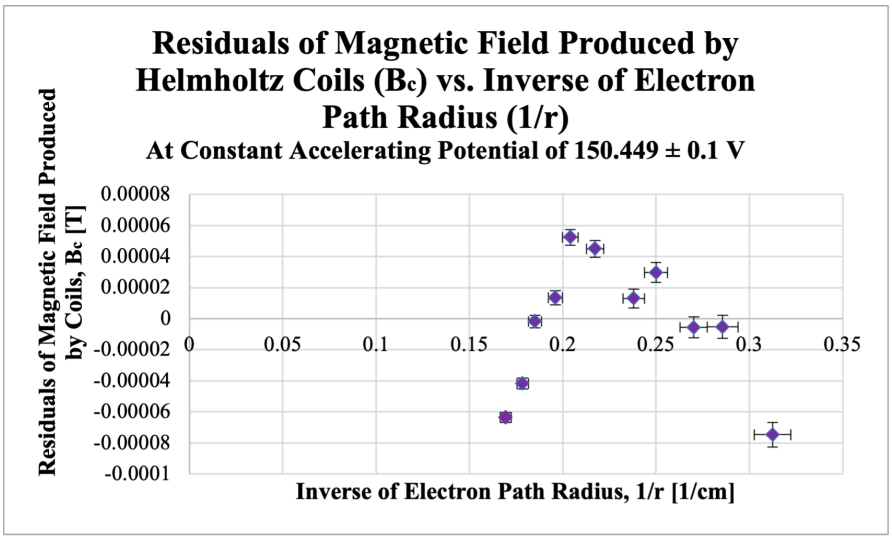

Figure 7: Scatter plot of residual coil-produced magnetic field B_c, against inverse of electron path radius, $\frac{1}{r}$, at a constant acceleration potential of 150.449 ± 0.1 V. The black vertical error bars represent the calculated uncertainty for B_c. The black horizontal error bars represent the calculated uncertainty for $\frac{1}{r}$ (Table 4).

The magnetic field of the Earth varies from 30 to 65 μT [2], hence an average of approximately 47.5 μT, which is significantly smaller (by a scale factor of $\frac{1}{7}$) than the calculated external magnetic field of $-0.32 \times 10^{-3} \pm 0.07 \times 10^{-3}$T). Because the external magnetic field is seven times larger than the Earth's average magnetic field, other sources contributed to the overall magnetic field acting on the electrons, which could affect the trajectory and accuracy of the readings. These sources include the magnetic field generated by other apparatus in the laboratory and electronic devices in the near vicinity.

4.4 Influence of Other Sources of Magnetic Fields

When ferromagnetic materials like cell phones and tablets were brought into the vicinity of the experimental set-up (between the Helmholtz coils), the radius of the electron beam decreased slightly, and the circular path became less uniform. This occurred because the presence of ferromagnetic materials distorted the uniformity of the magnetic field generated by the coils and introduced localized magnetic fields, which could lead to variation in the strength and direction of the field observed by the electrons.

However, this effect was only perceptible when the electronic devices were placed directly next to the glass bulb. Hence, this effect was not significant enough to impact the measurements as all other ferromagnetic

products, such as personal devices and apparatus, should be a significant distance away when conducting the experiment. Also, since the position of other ferromagnetic sources remained constant throughout the experiment, if they contributed to the external magnetic field, they did so throughout the entire experiment, meaning the measurements may not be accurate but were precise.

4.5 Charge-to-Mass Ratio, e/m

Using Equation 7 and 8 yields:

$$\frac{e}{m} = \frac{\Delta V}{r^2(kI + \frac{B_e}{\sqrt{2}})^2} \tag{12}$$

Where ΔV is the constant ΔV from Section 4.3 used to calculate the value of B_e, I and r^2 is the average of all measured currents and appropriate electron path radii squared, respectively, and k is given by:

$$k = \frac{1}{\sqrt{2}}(\frac{4}{5})^{3/2}\frac{(4\pi\times10^{-7}\text{T}\cdot\text{m}\cdot\text{A}^{-1})(130)}{0.16\pm0.001\text{m}} = 0.52\times10^{-3}\pm3.3\times10^{-6}\text{T}\cdot\text{A}^{-1} \text{ (Table 3, Equation 6)}$$

The charge-to-mass ratio of an electron is then:

$$\frac{e}{m} = \frac{150.449\pm0.1\text{V}}{(0.046\pm0.001\text{m})^2[(0.52\times10^{-3}\pm3.3\times10^{-6}\text{T}\cdot\text{A}^{-1})(1.206962\pm0.001\text{A})+\frac{-0.32\times10^{-3}\pm0.07\times10^{-3}\text{T}}{\sqrt{2}}])^2}$$

$$\frac{e}{m} = 0.41\times10^{12}\pm0.19\times10^{12}\,\frac{\text{C}}{\text{kg}}.$$

The literature value of $\frac{e}{m}$ is 1.759×10^{11} C kg^{-1} [3].

$$\%_{error} = \left|\frac{Literature\ Value - Experimental\ Value}{Experimental\ Value}\right|\times100 = \left|\frac{(1.759\times10^{11})-(0.41\times10^{12})}{0.41\times10^{12}}\right|\times100 = 57.09\ \%$$

Comparing the calculated value of the charge-to-mass ratio to the literature value, a percentage error of 57.09% is obtained, meaning there is a significantly large discrepancy between the literature and the calculated value of the charge-to-mass ratio, which could be a result of ferromagnetic interferences, variations in the external magnetic field, imperfect uniformity, and highly diffused circular beams formed at large currents and low voltages. These factors reduced the accuracy of the calculations.

References

[1] H. Zhan, E. Horsley, A. Harlick, "Charge-to-mass ratio for the electron." q.utoronto.ca. `https://q.utoronto.ca/courses/324674/files/27571481?module_item_id=5066346` (accessed Nov. 18, 2023).

[2] S. Hurley, "The Earth's magnetic field." explainingscience.org. `https://explainingscience.org/2016/04/24/the-earths-magnetic-field/#:~:text=The%20Earth's%20magnetic%20field%20is%20much%20weaker%20than%20this.,and%20weaker%20near%20the%20equator` (accessed Nov. 18, 2023).

[3] "Fundamental Physical Constants." physics.nist.gov. `https://physics.nist.gov/cgi-bin/cuu/Value?esme` (accessed Nov. 18, 2023).

[4] P. Bevington, D. Robinson, *Data Reduction and Error Analysis for the Physical Sciences*, 3rd ed. New York: McGraw-Hill 2003, pp. 65 - 71. Accessed: Nov. 18, 2023. [Online]. Available: `https://q.utoronto.ca/courses/324674/files/27381858?module_item_id=4988752`

Appendices

A Experimental Data

The fit and associated uncertainties for the relationships between coil current and radius, as well as accelerating potential and electron path radius, were determined using Excel's fitting programming, as seen in Figures **??** and 2. The fit was then employed to determine the residuals, producing Figures 5 and 3.
The reduced chi-squared values was calculated using the following equation [4]:

$$\frac{1}{N-m}\sum_{i=1}^{N}\frac{(r_i - r_{i,predicted})^2}{(\Delta r_i)^2} \tag{13}$$

where N is the number of data points, m is the number of fit parameters, r_i is the experimentally measured electron path radius, $r_{i,predicted}$ is the electron path radius as predicted by the fit, and Δr_i is the uncertainty in the electron path radius.

Table 1: Coil Current, I, vs. Electron Path Radius, r, at Constant Accelerating Potential of 150.449 ± 0.1 V

Current, $I, \pm 0.001$ (A)	Radius, $r, \pm 0.1$ (cm)	Fit-Predicted Value of r (cm) [2]	Residuals of Fit [3] (cm)
0.708617	5.9	5.90	-0.000
0.803370	5.6	5.64	-0.045
0.905003	5.4	5.37	0.030
1.003593	5.1	5.10	-0.004
1.113667	4.9	4.81	0.093
1.198239	4.6	4.58	0.022
1.301843	4.2	4.30	-0.098
1.409507	4.0	4.01	-0.008
1.505488	3.7	3.75	-0.048
1.615764	3.5	3.45	0.049
1.711487	3.2	3.19	0.008
1.206962	**4.6**	**4.55**	**0.000**

The bolded bottom row of Table 1 is the average of the above data.

Table 2: Accelerating Potential, ΔV, vs. Electron Path Radius, r, at Constant Current of 1.301142 ± 0.001 A

Accelerating Potential, $\Delta V, \pm 0.1$ (V)	Radius, $r, \pm 0.1$ (cm)	Fit-Predicted Value of r^2 (cm)	Residuals of Fit[3] (cm)
118.525	3.1	3.11	-0.006
140.009	3.3	3.38	-0.081
159.623	3.6	3.63	-0.032
180.974	3.9	3.91	-0.005
201.487	4.2	4.17	0.032
220.251	4.5	4.41	0.092
241.181	4.8	4.68	0.124
260.186	5.0	4.92	0.081
280.282	5.2	5.18	0.023
301.755	5.5	5.45	0.049
320.19	5.6	5.69	-0.087
341.367	5.9	5.96	-0.058

[2] With significant figure rules, this number should be reported to 1 decimal place. However, doing so would imply that the fit was nearly perfect. Hence, these values have been rounded to 2 decimal places.

[3] For reasons similar to above, these values have been rounded to 3 decimal places.

B Error Propagation and Calculated Data

The necessary uncertainties, Δ, for the values were calculated as in Table 3, with sample calculations. This propagation was followed to produce the uncertainties of all the relevant calculated values.

Table 3: Uncertainty Propagation of Different Values

Values	Uncertainty Formula	Sample Propagation
k	$\Delta k = \frac{\Delta R}{R} k$	For constant value of k: $\Delta k = \frac{0.001}{0.16}(\frac{1}{\sqrt{2}}(\frac{4}{5})^{3/2}\frac{\mu_0 n}{R})$ $\Delta k = \frac{0.001}{0.16}(\frac{1}{\sqrt{2}}(\frac{4}{5})^{3/2}\frac{(4\pi\times10^{-7}\text{T}\cdot\text{m}\cdot\text{A}^{-1})(130)}{0.16\pm0.001\text{m}})$ $\Delta k = \pm3.3\times10^{-6}\text{T}\cdot\text{A}^{-1}$
I_0	$\Delta I_0 = \frac{\Delta k}{k}\frac{B_e}{k} = \frac{\Delta k \cdot B_e}{k^2}$	For constant value of I_0: $\Delta I_0 = \frac{(\pm3.3\times10^{-6}\text{T}\cdot\text{A}^{-1})(-0.30\times10^{-3}\text{T})}{(0.52\times10^{-3})^2\text{T}\cdot\text{A}^{-1}}$ $\Delta I_0 = \pm3.7\times10^{-3}\text{A}$
$\frac{1}{r}$	$\Delta\frac{1}{r} = \frac{\Delta r}{r}\frac{1}{r} = \frac{\Delta r}{r^2}$	For $r = 5.9$ cm: $\Delta\frac{1}{r_{5.9}} = \frac{\pm0.1\text{cm}}{(5.9\text{cm})^2} = \pm0.003\text{cm}$
r^2	$\Delta r^2 = 2\frac{\Delta r \cdot r^2}{r} = \Delta r \cdot r$	For average value of $r = 0.046$ m: $\Delta r^2 = \pm0.001\text{m}\cdot0.046\text{m} = \pm0.000046\text{m}^2$
B_c	$\Delta B_c = \sqrt{\frac{\partial f}{\partial I}^2 + \frac{\partial f}{\partial R}^2}, f = (\frac{4}{5})^{3/2}\frac{\mu_0 n I}{R}$ $\Delta B_c = \sqrt{((\frac{4}{5})^{3/2}\frac{\mu_0 n}{R}\Delta I)^2 + (-(\frac{4}{5})^{3/2}\frac{\mu_0 n I}{R^2})\Delta R)^2}$ To calculate the uncertainty of B_c after the correction factor from Section 4.2.3 is applied, simply multiply the uncertainty value by the appropriate correction factor.	For $I = 0.708617$ A: $(\frac{4}{5})^{3/2}\mu_0 n \approx 1.17\times10^{-4}\text{T}\cdot\text{m}\cdot\text{A}^{-1}$ $\Delta B_c = \sqrt{(\frac{1.17\times10^{-4}}{0.16}(0.001\text{A}))^2 + (-\frac{(1.17\times10^{-4})(0.708617)}{0.16^2}(0.001\text{m}))^2}$ $\Delta B_c = \pm3.3\times10^{-6}$ T
$\frac{e}{m}$	$\Delta\frac{e}{m} = \sqrt{\frac{\partial f}{\partial\Delta V}^2 + \frac{\partial f}{\partial\Delta r}^2 + \frac{\partial f}{\partial\Delta k}^2\frac{\partial f}{\partial\Delta I}^2 + \frac{\partial f}{\partial\Delta B_e}^2}$, f = Equation 12	Uncertainty shown in Section 4.5

For Section 4.3, the formulae from Table 3 were applied to calculate the uncertainties. The axial distance ratio, $\frac{r}{R}$, where $r = \rho$, was calculated to determine what correction factor to use, as per Section 4.2.3. As all of the ratios were $0.2R < r < 0.5R$, the correction factor from Equation 10 was applied.

Table 4: Uncertainty Propagation and Calculated Data for Section 4.3

Electron Path Radius, $r, \pm0.1$ (cm)	Inverse of Electron Path Radius, $\frac{1}{r}$ (cm)	Coil Current, I, ±0.001 (A)	Coil-Produced Magnetic Field, B_c (T)	Axial Distance Ratio, $\frac{r}{R}$	Correction Factor	Corrected Coil-Produced Magnetic Field, B_c
5.9	$0.17 \pm 2.9\times10^{-3}$	0.708617	$5.2\times10^{-4}\pm3.3\times10^{-6}$	0.37	0.96	$5.0\times10^{-4}\pm3.2\times10^{-6}$
5.6	$0.18 \pm 3.2\times10^{-3}$	0.803370	$5.9\times10^{-4}\pm3.7\times10^{-6}$	0.35	0.97	$5.7\times10^{-4}\pm3.6\times10^{-6}$
5.4	$0.19 \pm 3.4\times10^{-3}$	0.905003	$6.6\times10^{-4}\pm4.2\times10^{-6}$	0.34	0.97	$6.4\times10^{-4}\pm4.1\times10^{-6}$
5.1	$0.20 \pm 3.8\times10^{-3}$	1.003593	$7.3\times10^{-4}\pm4.6\times10^{-6}$	0.32	0.98	$7.2\times10^{-4}\pm4.5\times10^{-6}$
4.9	$0.20 \pm 4.2\times10^{-3}$	1.113667	$8.1\times10^{-4}\pm5.1\times10^{-6}$	0.31	0.98	$8.0\times10^{-4}\pm5.0\times10^{-6}$
4.6	$0.22 \pm 4.7\times10^{-3}$	1.198239	$8.8\times10^{-4}\pm5.5\times10^{-6}$	0.29	0.99	$8.6\times10^{-4}\pm5.4\times10^{-6}$
4.2	$0.24 \pm 5.7\times10^{-3}$	1.301843	$9.5\times10^{-4}\pm6.0\times10^{-6}$	0.26	0.99	$9.4\times10^{-4}\pm5.9\times10^{-6}$
4.0	$0.25 \pm 6.3\times10^{-3}$	1.409507	$1.0\times10^{-3}\pm6.5\times10^{-6}$	0.25	0.99	$1.0\times10^{-3}\pm6.4\times10^{-6}$
3.7	$0.27 \pm 7.3\times10^{-3}$	1.505488	$1.1\times10^{-3}\pm6.9\times10^{-6}$	0.23	0.99	$1.1\times10^{-3}\pm6.9\times10^{-6}$
3.5	$0.29 \pm 8.2\times10^{-3}$	1.615764	$1.2\times10^{-3}\pm7.4\times10^{-6}$	0.22	0.99	$1.2\times10^{-3}\pm7.4\times10^{-6}$
3.2	$0.31 \pm 9.8\times10^{-3}$	1.711487	$1.3\times10^{-3}\pm7.8\times10^{-6}$	0.20	1.00	$1.2\times10^{-3}\pm7.8\times10^{-6}$